Unified Push Recovery Fundamentals: Inspiration from Human Study

Unified Push Recovery Fundamentals: Inspiration from Human Study

Christopher McGreavy, Kai Yuan, Daniel Gordon, Kang Tan, Wouter Wolfslag, Sethu Vijayakumar, Zhibin Li

***Abstract*— Currently for balance recovery, humans outperform humanoid robots that used hand-designed controllers. This study aims to close this gap by finding control principles which are shared across all recovery strategies. We do this by formulating experiments to test human strategies and quantify criteria for identifying strategies. A minimum jerk control principle is shown to accurately recreate human CoM recovery trajectories. Using this principle, we formulate a Model-Predictive Control (MPC) for the use in floating base systems (eg legged robots). The feasibility of generated motions from the MPC for implementation on the real robot is then validated using an Inverted Pendulum Model. Finally, we demonstrate improved capability over humans by tuning the parameters for time-optimal recovery performance.**

I. Introduction

This paper investigates push recovery in humans and robots. Push recovery is segmented into a set of discrete actions or modular strategies, each with a different method of control. In robotics, these discrete actions are used in two ways. One way is to use a strategy as a standalone push recovery controller [1], [2]. But this only tends to be useful against a small range of pushes. The other way is a unified approach. Using a single function to combine strategies is effective against a wider range of pushes [3], [4], but can require one strategy to transfer responsibility for the recovery motion to another [5]. Transfers between strategies, especially when each uses a different controller, can lead to failure cases. A second drawback is that users must select how much each action emerges during recovery [3]. Even with careful tuning, failures can occur when the tuned emergence ratios do not match the needs of the recovery.

In contrast, humans combine strategies into continuous motions [6]. In humans, strategies are used in many combinations [7] and are switched rapidly [8]. Thus it is unlikely that actions are chosen ahead of time or require different methods of control, especially when sensory delays are considered.

Motivated by this human behaviour, we hypothesise that the discrete actions share common fundamental principles which can be used as a common controller across all strategies. If found, these core principles could mean that all strategies can emerge from a single controller. This would be valuable for robotics by reducing the need to switch controllers when switching strategies. Also, fewer hyperparameters would be required and there would be no need to select how often each strategy should emerge.

This research is supported by the EPSRC as part of the CDT in Robotics and Autonomous Systems (EP/L016834/1).

The authors are with the Edinburgh Centre for Robotics and the School of Informatics, the University of Edinburgh, United Kingdom. Email: c.mcgreavy@ed.ac.uk

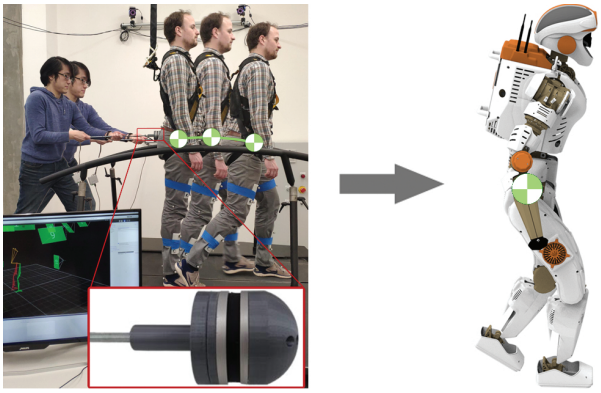

Fig. 1: Study of common principles in human push recovery that lead to better robot control policies.

A. Related Work

The discrete push recovery actions and their associated controllers are as follows:

Ankle Strategy regulates ankle torque to modulate the Centre of Pressure (CoP) to affect CoM (Centre of Mass) motions for small pushes. Observed in humans [7] and used legged robots [1], this strategy is effectively modelled by the Linear Inverted Pendulum Model (LIPM) [9].

Hip Strategy applies torque at the hip joint to induce angular momentum around the CoM. Though observed in humans [10] and applied to robotics [1] it is often overused despite its limited effectiveness [11].

Toe-Lift Strategy uses the toes to redirect horizontal CoM motion upwards and is prominent in human recovery [12]. Though robot toe-lift controllers exist [13] it is used less than other strategies due to difficulties during the under-actuated phase of the motion.

Step Strategy repositions contact points to shift the shape of the Support Polygon (SP) and is effective at halting the CoM, especially during large disturbances, therefore is prominently used in humans [6] and robots [2].

Discrete strategies can be combined using Model Predictive Control (MPC) [3]. However, parameters must be tuned to set the desired emergence of strategies, especially step strategy. Linear Quadratic Regulation [4] can effectively implement some strategies by minimising joint deviations but does not include step strategy. Using a Proportional Integral Derivative (PID) allows ankle and step strategies to emerge naturally on a real robot [14]. A Quadratic Programming (QP) whole-body controller was used to solve the joint angles. This is a reasonable approach considering QP controllers are likely to already being used in many robots.

TABLE I: Threshold values for determining when strategies are active.

Action	Criteria	Threshold	Human Max	Unit	Method
CoP	$p_{\text{heel,z}} \leq \delta_{\text{heel,z}}$	$\delta_{\text{heel,z}} = 0.01$	Variable	m	N/A
Angular Momentum	$L_t > \delta_t$	$\delta_t = 0.1$	0.49	s(Normalised)	Torso sway with feet fixed to ground
CoM Height	$\dot{z} > \delta_{\dot{z}}$	$\delta_{\dot{z}} = 0.02$	0.1269	m/s	Stand on toes as quickly as possible
Support Polygon	$p_{\text{toe,z}} > \delta_{\text{s},v_{\text{L,R}}} > \delta_{\text{s}}$	$\delta_{\text{s}} = 0$	N/A	N/A	N/A

Notation: $p_{\text{heel,z}}$ Heel height, L_t Hip Angular Momentum, $\dot{z}$ CoM Velocity (Z Axis), $p_{\text{toe},z}$ Toe Height, $v_{\text{L,R}}$ Foot Velocity (X Axis) $\delta_{\text{heel,z}}$ Heel Height Threshold, δ_t Hip Angular Mom. Threshold, $\delta_{\dot{z}}$ CoM Height Threshold, δ_s Step Threshold

As we have seen, strategies tend to appear simultaneously in humans [15], [8]. We investigate this behaviour aiming to find shared principles of push recovery strategies. Applying this principle to robotics could reduce the number of parameters needed to tune recovery behaviour, since strategies would emerge naturally. To investigate these common principles, we first collect data of humans recovering from pushes. Data will be analysed to extract any common principles which may exist between the strategies. We then investigate how any principles might be adapted to use in robotics.

B. Contributions

This work presents the following contributions:

1) A concrete experimental design to extract useful physical quantities from human study to identify recovery strategies in humans
2) A set of criteria that allow the classification of push recovery strategies in humans
3) Evidence to show that a single model combined with a unified minimum jerk control principle explains human CoM motion as core strategies during push recovery
4) A controller based on these minimum jerk principles that can produce desirable performance and resemble human CoM behaviour to an extent
5) A controller tuned using these core principles which produces CoM motions similar to humans, but with better performance.

This paper is structured as follows. We describe our experimental method for data collection in Section II, then define a set of criteria for identifying recovery strategies and show their relationship (Section III). Using this data, Section IV presents the methodology to discover an underlying model to explain the CoM data. Section V shows the results of the search for a unifying principle and a validation study by implementing those principles on a balance controller. We then make conclusions in Section VI based on our findings.

II. Experimental Setup and Data Collection of Human Experiments

This section describes the experiments that capture human push recovery behaviours. These allow us to understand human push recovery, identify control parameters and obtain a baseline controller performance.

A. Subjects

60 recovery trials were collected from 4 participants recruited from the University of Edinburgh. Ethics approval was granted and each participant gave written informed consent before trials began.

B. Equipment

A mounted force/torque sensor (Fig. 1 inset) was used to push subjects and measure the applied force. VICON motion tracking recorded the movement of optical markers. A template of human body mass distribution was scaled to each participant in OpenSim [16]. This was used to calculate CoM position, joint angles and positions in gait analysis tools [17]. Body dimensions used to calculate angular momentum were obtained in the same way.

C. Experimental Design

15 push trials were performed on each participant. Each was instructed to try to return to the initial position after the push unless a step was required. If stepping was required, instructions were to come to a stop and not attempt to return to the initial position. Illustrated in Figure 1, participants were pushed at the coccyx using the force/torque device. Pushes were applied after 2-3s of quiet standing. Subjects did not know exactly when pushes would be applied nor their magnitude. After the push was complete the subject took a recovery action. To ensure subject response was purely reactionary, pushes were applied by experimenters. This reduced any sensory clues giving away the start of the push. Pushes applied to include a wide spectrum of impulses and whilst ensuring subject safety. Impulses ranged from $12.1\frac{\text{N}}{\text{s}}$ to $55.5\frac{\text{N}}{\text{s}}$, with a mean and standard deviation of $35.9\frac{\text{N}}{\text{s}}$ and $10.3\frac{\text{N}}{\text{s}}$.

D. Data Considerations and Post Processing

Recovery begins after the push force is removed and ends when stability is regained. As such, motion capture data is trimmed to remove movement when force sensor readings are below 2N and data after recovery has ended. Subjects were pushed forwards, resulting in minimal lateral movement. Thus only sagittal movement is considered. Velocity, acceleration and jerk were obtained by differentiating marker positions over the control frequency of the VICON motion capture. CoM states are normalised by leg length, thus are unitless. Low-pass filtering was applied to denoise all data (4th order Butterworth, cut-off frequency at 6Hz).

III. Strategy Identification Criteria

To identify the strategies present in the data, we formulate a set of criteria and thresholds. These criteria clearly determine the active component(s) of a strategy (Table I).

Since multiple recovery strategies simultaneously, we use the nomenclature of *Control Actions* and recovery *Strategies* to distinguish between discrete methods of recovery and a label for an entire recovery trial respectively. The discrete

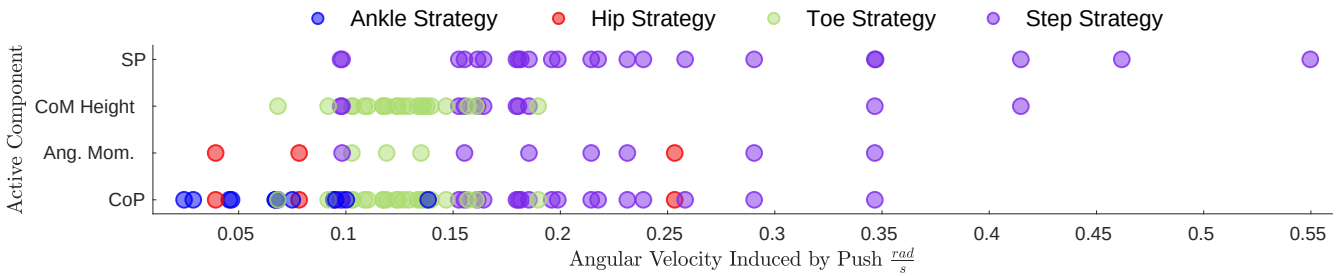

Fig. 2: Active components of strategies (y axis, circles) appear at different frequencies depending on the angular velocity (CoM w.r.t the ankle) caused by a push. Each colour shows which main strategy is used in that trial. Vertically aligned circles also represent a single trial, though connecting lines were removed for visibility.

push recovery actions discussed in Sec. I-A are all based on a single active component. For example, the active component of the ankle strategy is manipulating the CoP. The criteria in Table I can then be used to identify which control actions are active at each timestep of a recovery trial. *Strategy* labels denote the highest *Control Action* that was used during a trial. Control Actions ranks are determined by the maximum normalised impulse rejected during each trial (Table II). By making this distinction, we can qualitatively investigate how humans perform push recovery. This will add to the evidence that humans are unlikely to pre-select discrete recovery motions or use different policies to control them. The mean CoM trajectories for each Strategy are plotted in Figure 5.

TABLE II: Max normalised impulse observed in each action.

Rank	Action	Impulse [ms]
1	CoP Modulation	52
2	Angular Momentum Modulation	59
3	CoM Height Modulation	72
4	SP Modulation	77

A. Relationship Between Control Actions and Push Recovery Strategies

Figure 2 shows how control actions are used as characteristics of the push changes. In this case, the push magnitude is represented by the angular momentum w.r.t subjects' ankles, as caused by the push. We see that Control Actions are used in different ways depending on the push magnitude. Lower ranked actions tend to be used for smaller pushes and are gradually combined as the magnitude increases. For the largest pushes, weaker actions are skipped altogether and subjects immediately resort to higher ranked actions. Since subjects are unable to predict the push force in advance, it is logical to gradually employ increasingly more effective techniques to complete the recovery.

Figure 3 illustrates this relationship, showing that as the subject strays further from the equilibrium (*i.e.* quiet standing), stronger Control Actions (blue boxes) are used. Once the bulk of the recovery motion is complete, lower Control Actions are used to fine-tune the body position.

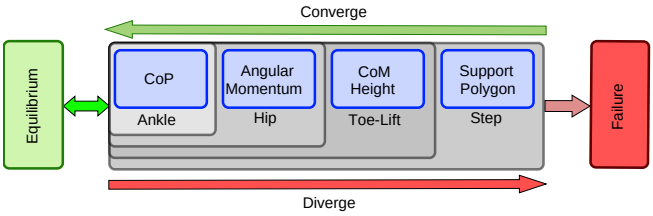

Fig. 3: Relationship between control actions and strategies. As a system diverges from the equilibrium, a sequence of control actions (blue) will be activated. A strategy is defined by the highest active/dominant control action (grey gradient).

B. Stability regions

Having established the relationship between the Control Actions in humans, we can begin to identify how effective they are and when they might be used. We do this by calculating a set of stability regions. These regions represent the actions which can affect the CoM in a given state. We calculate these regions for humans and for an example robot. The physical values we use for both are shown in Table III. Robot values use the specifications of the Valkyrie robot, whereas human values are obtained experimentally.

By adding physical constraints to a subject, we were able to sequentially isolate the effect of each action. CoP modulation parameters required only a mean foot length among participants. For angular momentum modulation, $\tau_{\max}$ a participant's heels were fixed to the ground and they were told to only use their hip to recover. Increasing push forces were applied to the CoM until recovery using the hip was no longer possible. CoM Height Modulation parameters were the same as those in Section III. For Support Modulation parameters increasing pushes were applied to the CoM until a flight phase was required for recovery. $v_{\max}$ is the foot max foot velocity of the push before the flight phase was used.

The stability region is defined according to CoM initial state $\boldsymbol{x}_0 = [x_0, \dot{x}_0]$. An action is able to stabilise the system if $\boldsymbol{x}_0$ is in the stability region, which is calculated for each action as follows. Results are shown in Figure 4.

1) CoP Modulation: To remain stable whilst balancing, the CP must lie within the Support Polygon:

$$p_{\min} \leq x + \omega \dot{x} \leq p_{\max}, \tag{1}$$

TABLE III: Physical properties required for calculating balance limits and their associated boundaries.

	COP Modulation		Angular Momentum Modulation		COM height Modulation		Support Polygon Modulation		
	$p_{\min}$ [m]	$p_{\max}$ [m]	$\theta_{\max}$ [rad]	$\tau_{\max}$ [Nm]	$v_{z,\max}$ $[\frac{\text{m}}{\text{s}}]$	$z_{\max}$ [m]	Step Length [m]	$v_{\min}$ $[\frac{\text{m}}{\text{s}}]$	$v_{\max}$ $[\frac{\text{m}}{\text{s}}]$
Human	0.10	0.17	0.27	3.01	0.13	0.13	0.5	0.1	3.95
Robot	0.12	0.19	0.66	150	0.10	0.07	0.25	0.1	3.00

where $\omega = \sqrt{g/z_c}$, and foot dimension (support polygon bounds) $p_{\min}, p_{\max}$. This bound is more practical than the ZMP criterion [18] since the CoM must be within the SP at the end of the recovery (at $t \to \infty$). The CP can then be controlled by modulating the CoP within the SP using the dynamics of the LIP model [9].

2) Angular Momentum Modulation: Extending CoP Modulation this action allows additional control via torque around the CoM, thus expanding the Capturability Region [2]:

$$p_{\min} - \alpha \leq x + \omega\dot{x} \leq p_{\max} + \alpha, \tag{2}$$

with $\alpha = \frac{\tau_{\max}}{\beta^2 mg}(\beta - 1)^2$, $\beta = e^{\omega T_{\max}}$, mass m, gravity constant g, maximal torso actuator torque $\tau_{\max}$, $\omega = \sqrt{g/z_c}$, maximum time $T_{\max} = \sqrt{4I/\tau_{\max}(\theta_{\max}) - \theta_0)}$, inertia I, maximal torso angle $\theta_{\max}$ and starting angle θ_0.

3) CoM Height Modulation: This control action increases virtual leg length, e.g., through toe-tilting, and provides a force f perpendicular to the COM velocity that reduces the horizontal velocity $\dot{x}$. To find the Stability Region for toe-tilting we need to analyse whether horizontal CoM velocity can be reduced to zero at the edge of the foot.

The horizontal velocity $\dot{x}_0$ is induced by external pushes, while the vertical velocity $\dot{z}(x_0, \dot{x}_0)$ can be added through CoM Height Modulation. We assume that COM motion will follow a straight line from initial condition $[-x_0, z_c]$ to endpoint $[0, z_c + \Delta z_{\max}]$. This over-approximates the Stability Region by assuming that the required force f can be generated at all times. For a more conservative estimation, a stability margin for the endpoint can be set instead of letting it be at the edge of the foot. To achieve a straight line, a vertical velocity $\dot{z}$ needs to be set:

$$\dot{z}(x_0, \dot{x}_0) = \sqrt{\frac{\Delta z_{\max}^2 \dot{x}_0}{(x^2 + \Delta z_{\max}^2)(1 - \frac{\Delta z_{\max}^2}{x_0^2 + \Delta z_{\max}^2})}}, \tag{3}$$

while not exceeding the physical capabilities of the robot:

$$\dot{z}(x_0, \dot{x}_0) \leq \dot{z}_{\max}. \tag{4}$$

Due to f being perpendicular to the COM velocity, we can energy balance to compute velocity at the foot edge. At this point $E_{\text{kinetic}} \leq \Delta E_{\text{potential}}$ must hold with $E_{\text{kinetic}} = \frac{1}{2}m(\dot{x} + \dot{z}(x_0, \dot{x}_0))^2$, and $\Delta E_{\text{potential}} = mg\Delta z_{\max}$. If this constraint is not met, the robot will pivot around the toe and fall if no further control action is taken.

4) Support Polygon Modulation: The Support Polygon Modulation (stepping) stability region is determined by running the controller proposed in Section IV-B.2 with the given initial CoM state. If for the given initial condition, the robot can come to a halt using the given constraints on step velocity and step length, then this initial condition is assumed to be within the stability region.

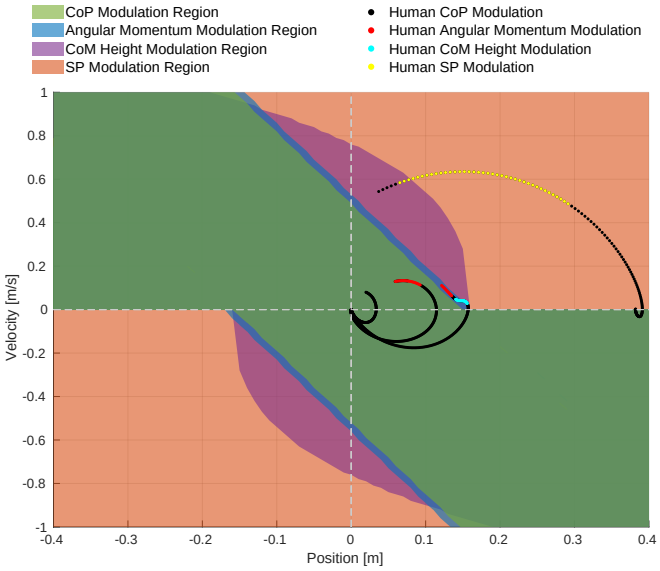

Fig. 4: Stability regions for each action to show how each affects CoM behaviour. The coloured curves show human CoM motion during recovery trials and are coloured according to which action is being used.

Figure 4 shows these stability regions in relation to human CoM trajectories and Control Actions. The approximate stability regions are a close match to the Actions (coloured dots) shown in human movement. In the non-stepping cases, the CoM remains in the original support polygon, whereas in the stepping case, the CoM diverges to a new SP.

IV. CoM Behaviour During Recovery Strategies

Here we investigate if a single control principle is shared across push recovery trials. This principle should be able to exhibit all uncovered push recovery strategies without needing a switching mechanism between the Control Actions.

A. CoM Modelling

The human motion analysis shows the dominating effects of the CoM dynamics. Hence a point mass model will be used to analyse human CoM data and to find the fundamental principles between the strategies The CoM model is able to freely move both horizontally and vertically.

Depending on the controller, we use a double integrator or triple integrator model to fit human data:

$$\frac{\mathrm{d}^2}{\mathrm{d}t^2}x = u, \tag{5}$$

$$\frac{\mathrm{d}^3}{\mathrm{d}t^3}x = u, \tag{6}$$

where x is CoM position and the controlled variable u is either CoM acceleration $\ddot{x}$ or jerk $\dddot{x}$. The model assumes the required control input u can be produced by the Ground Reaction Forces (GRF). This assumption will be ensured by constraining the input in the MPC. An independent integrator model is used for each axis, horizontal and vertical.

B. Identifying Control Principles: Formulations

Our aim is to find a single control principle which can accurately match the measured human trajectories in all strategies. We formulate candidates for these principles below.

1) PD & PID Control Formulation: The first candidates are Proportional Derivative (PD) and Proportional Integral Derivative (PID) feedback controllers. This is motivated by the simplicity of the human CoM trajectories. PID control is formulated below. The PD formulation is obtained by setting $K_i = 0$:

$$u(t) = K_p(e(t)) + K_d(\dot{e}(t)) + K_i \int_0^t e \, \mathrm{d}t, \tag{7}$$

where $e = x_{\text{des}}(t) - x(t)$, $\dot{e} = \dot{x}_{\text{des}}(t) - \dot{x}(t)$ is the error between the current position and current velocity respectively. x,$\dot{x}$,x_{des},$\dot{x}_{\text{des}}$ represent the position and velocity of the CoM and the desired position and velocity respectively. There will be one PD controller for each axis.

2) Model-Predictive Control Formulation: A minimum jerk principle is also used as a candidate to fit the human CoM motions. The strong resemblance between the human data and minimum jerk trajectories often used to explain human motions [19] motivates this decision. A minimum jerk MPC controller is designed, which minimises the objective function:

$$C(u(t)) = \frac{1}{2}\int_0^{t_f} \left(\frac{\mathrm{d}^3 x(t)}{\mathrm{d}t^3}\right)^2 dt = \frac{1}{2}\int_0^{t_f} u(t)^2 \mathrm{d}t. \tag{8}$$

Jerk $\frac{\mathrm{d}^3 x}{\mathrm{d}t^3}$ is used as control effort u with final time t_f. The MPC solves the following constrained optimisation problem:

$$\min_{u(t)} \quad C(u(t))$$

subject to Eq. 5

$$[x(0), \dot{x}(0), \ddot{x}(0)] = [x_0, \dot{x}_0, \ddot{x}_0] \tag{9}$$

$$[x(t_f), \dot{x}(t_f), \ddot{x}(t_f)] = [x_f, \dot{x}_f, \ddot{x}_f] \tag{10}$$

$$[x_{\min}, \dot{x}_{\min}, \ddot{x}_{\min}] \leq [x, \dot{x}, \ddot{x}] \leq [x_{\max}, \dot{x}_{\max}, \ddot{x}_{\max}], \tag{11}$$

with initial condition $[x_0, \dot{x}_0, \ddot{x}_0]$, and terminal condition $[x_f, \dot{x}_f, \ddot{x}_f]$. Equation 11 represents the physical feasibility to be shown in Section V-B.

C. Minimum Jerk Model Predictive Control (MJMPC)

The MJMPC scheme is detailed in Algorithm 1. First, the desired CoM states X_{des}, Z_{des} are set as terminal conditions in the constrained optimisation problem. While the desired CoM height stays constant, the desired horizontal CoM x_d is computed by the step optimiser (Section IV-D.2) if the CP exceeds the SP. Additionally, using the current state as the initial condition X_0, Z_0 and the final time t_f (Section IV-D.3), the control effort $u_{x,1:t_f}, u_{z,1:t_f}$ is then calculated over prediction horizon t_f by solving the constrained optimisation (9). Lastly, a whole-body QP controller calculates feasible and realisable joint torques τ by executing the first CoM reference position gained by minimising CoM jerk value $X_{\text{ref}} \leftarrow X_{\text{ref},1:t_f}(1)$ from the whole control input trajectory $u_{i,1:t_f}$ in an MPC fashion.

Algorithm 1 Algorithm for MJMPC

$X_{\text{des}} \leftarrow [0,0,0]^T$, $Z_{\text{des}} \leftarrow [z_c,0,0]^T$
while $X \neq X_{\text{des}}$ **do**
  if $CP > SP$ **then**
    $X_{\text{des}} \leftarrow step\_optimiser(X)$
  end if
  $X_0 \leftarrow X$, $Z_0 \leftarrow Z$
  $X_{\text{ref}} \leftarrow \min_{u(t)} f(u(t))$
  $X_{\text{ref}} \leftarrow X_{ref,1:t_f}(1)$
  $Z_{\text{ref}} \leftarrow \min_{u(t)} f(u(t))$
  $Z_{\text{ref}} \leftarrow Z_{ref,1:t_f}(1)$
  $\tau \leftarrow$ Whole Body Control($X_{\text{ref}}, Z_{\text{ref}}$)
  $X, Z \leftarrow$ Robot(τ)
end while

Although the Angular Momentum Modulation was present in the human data, its contribution to overall push recovery is so minor [11] that it can be exempted in the current model.

D. Optimising Parameters to Fit Human Data

Three components are required before these controllers can be fitted to human trajectories: initial condition $\boldsymbol{x}_0$, terminal condition $\boldsymbol{x}_f$ and hyperparameters of each controller.

1) Initial Conditions: For each experimental trial, we are interested how humans reactively recover from pushes, so we only consider CoM movement after the push force is removed until recovery is achieved. As such, each controller will be fit to each human trial using the CoM state at the moment the push is removed at the initial condition $\boldsymbol{x}_0$ for each trial. States are determined by the equations of motion in Equations 5 and 6.

2) Terminal Conditions: The reference state $\boldsymbol{x}_f = [0,0,0]^T$ as the terminal condition is applied to all non-stepping actions. For stepping actions, a new CoM reference is required, which is provided by an optimisation method for foot placement [20]. This step optimisation considers kinematic and dynamic limits of the physical system as inequality constraints and outputs a new step location which is the final CoM position x_d, yielding the terminal constraint as $\boldsymbol{x}_f = [x_d, 0, 0]$. A step is only taken when the CP of the system is beyond the SP. Our collected human data only involve a single step, but this can be extended to multiple steps for large pushes.

3) Final Time: The hyperparameters for each controller are determined via the least square fitting. The fitting minimises the least square error between the CoM trajectory gen-

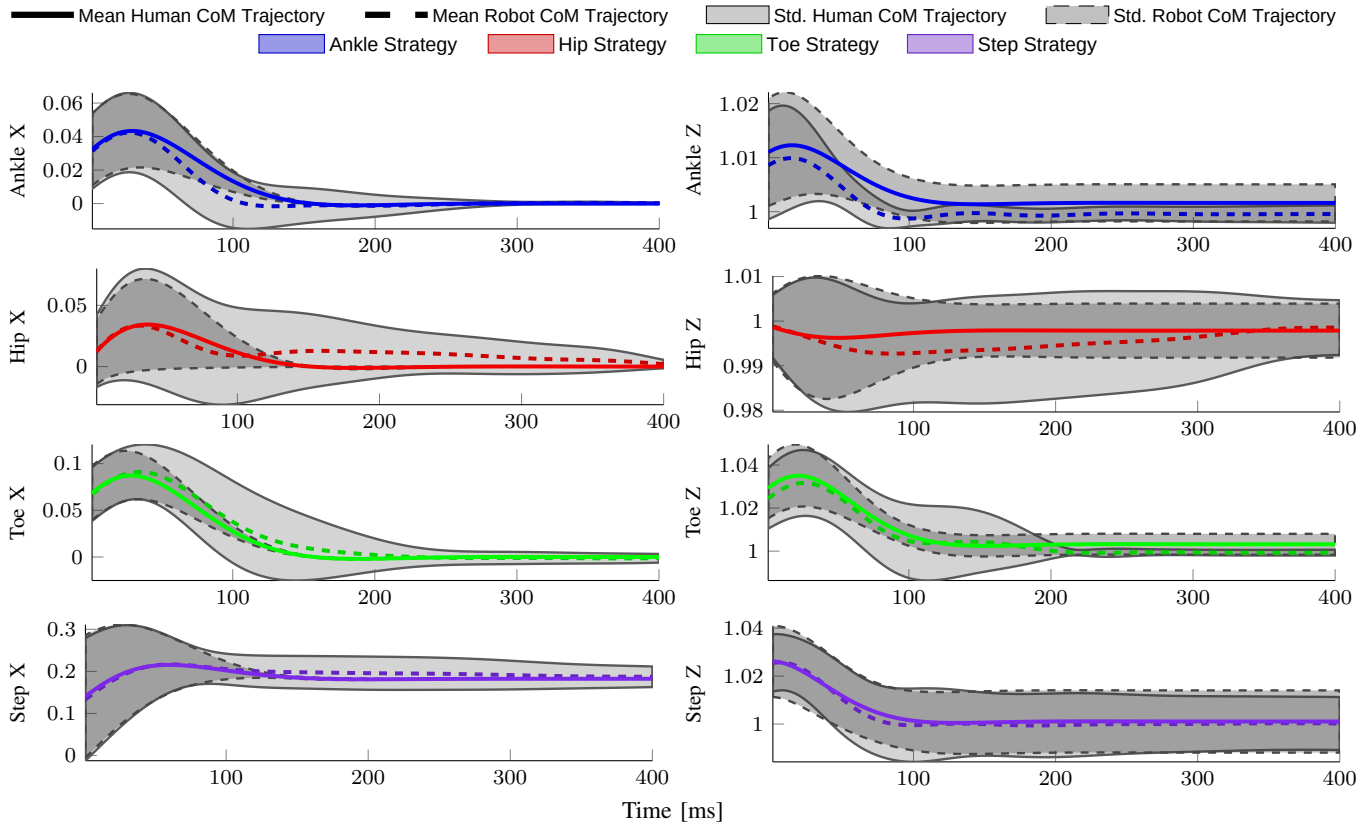

Fig. 5: Comparison of human (solid line) and robot (dashed line) performance. Rows: ankle, hip, toe, step strategies in X and Z axes (columns). Units: leg length l.

TABLE IV: Comparing model fits & human trajectories.

	Axis	Mean MSE in [mm^2] Ankle	Hip	Toe	Step	Total
Min Jerk	X	0.022	0.075	0.623	0.560	0.366
	Z	0.003	0.005	0.07	0.01	0.0257
PD	X	0.063	0.538	0.268	3.218	1.371
	Z	0.004	0.027	0.042	0.052	0.037
PID	X	0.071	0.504	0.236	3.136	1.328
	Z	0.004	0.028	0.041	0.082	0.049

erated by humans Y and controller Y^*, given the controller-specific parameters P at each time step t:

$$\sum_{i=1}^{N}\sum_{t=1}^{T}(Y^*_{t,i}(P) - Y_{t,i})^2. \tag{12}$$

Optimisation was performed using the MATLAB `fmincon`, and t_f was fit to both the X and Z axes for all trials.

V. Results

In this section we present the results of fitting PD, PID and MJMPC controllers to the human data collected in Section II. We then analyse the feasibility of the generated motions and their stability regions.

A. Characterising Human Data

In section IV-D.3, we optimised parameters P for each controller to match human CoM trajectories as closely as possible. Table V shows the parameters which gave the closest match to human CoM trajectories. We implemented each controller in the X & Z axis using the point-mass models derived in Section IV-A. Initial and final parameters shown in Section IV-D were used. This results in a new set of trajectories created by these controllers which attempt to match the real human CoM movements in all strategies as closely as possible. Figure 5 and Table IV show the results. In Figure 5 we superimpose the trajectories from the best fitting controller, the MJMPC (dotted lines) onto the mean human CoM trajectories (solid lines) for each strategy. The overlap of human trajectories with the mean robot trajectories generated from MJMPC shows that the MJMPC is able to closely characterise the human policy obtained from experiments.

Table IV shows the Mean Squared Error (MSE) for the MJMPC, PD and PID models. The MJMPC has the lowest MSE in both the X & Z axes, with a total MSE over all trials of 0.366mm^2 and 0.0257mm^2 respectively. More importantly, the MSE between the MJMPC and the human CoM trajectories is consistently low across all strategies.

TABLE V: Parameters used to match human CoM behaviour.

Axis	MJ Param. Time Horizon [ms]	PD Params K_P	K_D	PID Params K_P	K_D	K_I
X	123	71.4	31.7	63.8	68.9	1.4
Z	101	146.9	67.1	0.1	28	0

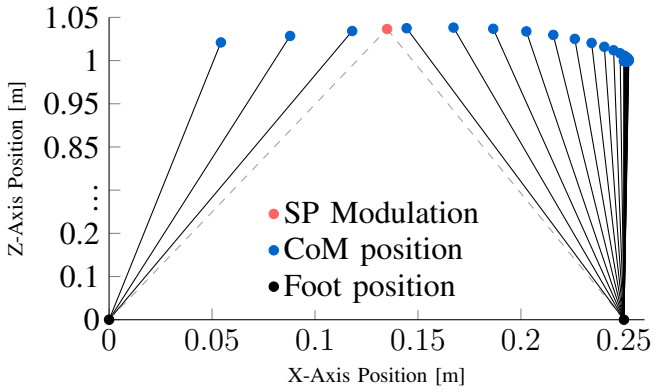

Fig. 6: Time-elapsed CoM behaviour for step strategy using the MJMPC controller.

MSE data for the PD and PID controllers are slightly higher than the MJMPC. This means that the MJMPC can be considered an effective principle to account for human CoM motions regardless of which strategy is being used.

B. Stability and Feasibility Analysis of MJMPC

Despite the constraints of the CoM motion in the MPC, infeasible motions may still occur if the boundaries are determined wrongly. Therefore, an analysis regarding the stability regions of the system and consideration of the joint torque limits is conducted.

We validate the feasibility of the calculated CoM trajectory using an Inverted Pendulum Model (IPM) to ensure that the trajectory can be achieved, as detailed in Appendix A The max force and torque used during these trajectories is 1384N and 352Nm respectively. This is well within the Valkyrie specifications: $f_{\max} = 2500$N, $\tau_{\max} = 1000$Nm. We show the time elapsed illustration of the performed IPM simulation is shown in Figure 6.

C. Applying Push Recovery Principles to Robotics

Now we've shown that a single control principle can be used to explain human CoM motion across the four main push recovery strategies, we can look into how this can be used for robotics. In the earlier section, we tuned the parameter of our MJMPC controller to match human performance. Our goal, however, is not to blindly imitate human behaviour. Our real aim is to extract useful principles from human behaviour such that they can be used in robotics. If we use the same controllers we used in the previous section, but this time tune the parameters such that the CoM reaches the desired state as quickly as possible, we may obtain better performance. This time, parameters were tuned using a time-optimal like control cost, subject to force and torque limits of our example robot in Table III:

$$\min_{x(t),z(t)} \quad \frac{1}{2}\int_0^{t_f} ((x_d(t)-x(t))+(z_d(t)-z(t)))^2 \mathrm{d}t \quad (13)$$

$$\text{subject to:} \quad \tau \leq \tau_{\max} \quad (14)$$

$$F \leq F_{\max} \quad (15)$$

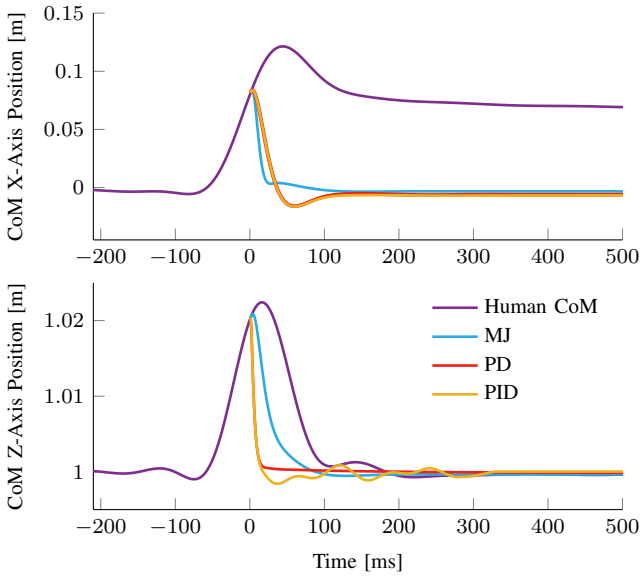

Fig. 7: Mean CoM trajectories from an extended version of the control principles, tuned for time optimal performance. In the X Axis, the PD and PID curves are almost identical. All controllers converge to the desired position faster than humans. Furthermore, due to faster responses controllers do not require a step to recover from the push. Time (X-Axis) is reset as zero when the push ends.

where $x(d), z(d)$ are the desired positions for the controller, set to the initial position of the human CoM during quiet standing before the push starts. If the CP moves out of the SP, the same step selection criteria as in IV-D were used.

Figure 7 shows the performance of each controller using the new parameters. The mean human CoM behaviour for all trials collected in the study is also plotted for comparison. We see in this figure that the mean human trajectory after being pushed diverges significantly from the initial position, caused by human subjects taking a step. In contrast, each controller is able to return to the initial position without stepping, since the calculated CP does not move outside the SP (Alg:1, Ln:3).

When we were fitting the controllers to the human CoM trajectories in the previous section, the controllers were implicitly accounting for sensing and muscle actuation delays in humans. Since these delays are trivial in robotics, using this time optimal approach, we can achieve higher performance than in the human data.

D. Comparing Stability Region between Human and Robots

The boundaries defined in Section III-B are used to generate stability regions for robots (Fig. 8) using the values in Table III. The robot stability regions are qualitatively similar to human regions in 4. Furthermore, the low effectiveness of Angular Momentum Modulation can be seen through its stability region in both human and robot plots. It largely overlaps with the CoP Modulation, and in most cases is within the CoM height modulation stability region. This indicates that the Angular Momentum Modulation is, in fact, replaceable by a combination of CoP and CoM Height

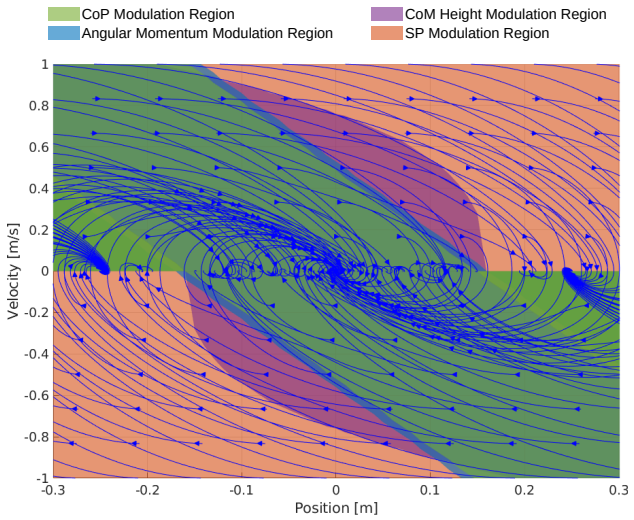

Fig. 8: Regions of attraction for our control principle with respect to the stability regions in Section V-D. Arrows show the trajectories of controlled motion from a grid of initial conditions, which stray into the stepping region converge at step locations calculated in Section IV-D.

modulations, and human data was indeed well reconstructed using this approach as shown in Section V-A.

VI. Conclusion

This paper first investigated human push recovery motions. We quantified a set of criteria which can identify when Control Actions are being used. Once these were identified, we were able to find a common minimum jerk control principle which could accurately match each of these Control Actions. Taking this control principle, we were then able to increase performance by tuning its parameters to perform optimally rather than to fit human data.

From this, we conclude that despite the apparent complexity of human recovery behaviour, by focusing on the CoM, a simple core rule can account for the wide variety of motion. In studying human push recovery, we obtain a warm-start to show effective ways of exploring complex movement problems in robotics. Adapting these principles also has value in robotics. As a next step, we will validate feasible recovery motions on a real system performed by the controller while undergoing a series of pushes. Furthermore, future work will study more complex motor skills from humans, such as fall recovery and climbing, and investigate new framework and approaches to transfer more human-level skills to robots.

Appendix

A. Stability and Feasibility Analysis of MJMPC

Max possible force $f_{\max}$ and torques $\tau_{\max}$ are calculated considering the joint torque limits $\boldsymbol{\tau}_{\lim}$. For every joint state $Q = [q, \dot{q}, \ddot{q}]^T$, the maximal admissible ground reaction wrench $\lambda_{\lim} = [f_{\max}, \tau_{\max}]^T$ are calculated via inverse dynamics as:

$$M(q)\ddot{q} + c(q,\dot{q}) + g(q) = \begin{bmatrix} 0_{6\times n} \\ I_{n\times n} \end{bmatrix} \boldsymbol{\tau}_{\lim} \tag{16}$$

$$\Rightarrow \lambda_{i,lim} = J_i(q)^{T\#}(M(q)\ddot{q}+c(q,\dot{q})+g(q)-\begin{bmatrix} 0_{6\times n} \\ I_{n\times n} \end{bmatrix} \boldsymbol{\tau}_{\lim}), \tag{17}$$

where $J(q)^{T\#}$ is the pseudo inverse of the Jacobian for ith foot, $M(q)$ is the inertia matrix, $c(q,\dot{q})$ non-linear effects, and $g(q)$ the gravity component.

References

[1] B. Stephens, "Humanoid push recovery," in *IEEE-RAS Int. Conf. on Humanoid Robots*, 2007.

[2] J. Pratt, *et al.*, "Capture point: A step toward humanoid push recovery," in *IEEE Int. Conf. on Humanoid Robots*, 2006.

[3] Z. Aftab, *et al.*, "Ankle, hip and stepping strategies for humanoid balance recovery with a single model predictive control scheme," in *IEE Int. Conf. on Humanoid Robots 2012*.

[4] C. G. Atkeson and B. Stephens, "Multiple balance strategies from one optimization criterion," in *IEEE Int. Conf. on Humanoid Robots 2007*.

[5] L. Kaul and T. Asfour, "Human Push-Recovery:Strategy Selection Based on Push Intensity Estimation," *Int. Symp. on Robotics*, 2016.

[6] H. Hoffmann, *et al.*, "Biologically-inspired dynamical systems for movement generation: Automatic real-time goal adaptation and obstacle avoidance," *IEEE Int. Conf. on Robotics and Automation 2009*.

[7] L. M. Nashner and G. McCollum, "The organization of human postural movements: a formal basis and experimental synthesis," *Behavioral and brain sciences*, 1985.

[8] Y.-C. Pai and J. Patton, "Center of mass velocity-position predictions for balance control," *Journal of biomechanics*, 1997.

[9] S. Kajita and K. Tani, "Study of dynamic biped locomotion on rugged terrain-derivation and application of the linear inverted pendulum model," *IEEE Int. Conf. on Robotics and Automation*, 1991.

[10] J. Allum and F. Honegger, "Interactions between vestibular and proprioceptive inputs triggering and modulating human balance-correcting responses differ across muscles," *Experimental brain research*, 1998.

[11] P. Zaytsev, *et al.*, "The boundaries of walking stability: viability and controllability of simple models," *IEEE Trans. on Robotics*, 2018.

[12] K. B. Cheng, *et al.*, "Role of heel lifting in standing balance recovery: A simulation study," *Journal of Biomechanics*, 2018.

[13] Z. Li, *et al.*, "Humanoid balancing behavior featured by underactuated foot motion," *IEEE Transactions on Robotics*, 2017.

[14] K. Seo, *et al.*, "Towards natural bipedal walking: Virtual gravity compensation and capture point control," in *IEEE Int. Conf. on Intelligent Robots and Systems*, 2012.

[15] A. Hofmann, "Computer Science and Artificial Intelligence Laboratory Technical Report Robust Execution of Bipedal Walking Tasks From Biomechanical Principles," 2006.

[16] S. L. Delp, *et al.*, "Opensim: open-source software to create and analyze dynamic simulations of movement," *IEEE transactions on biomedical engineering*, 2007.

[17] D. Gordon, *et al.*, "Effectively quantifying the performance of lower-limb exoskeletons over a range of walking conditions," *Frontiers in Robotics and AI*, 2018.

[18] S. Kajita, *et al.*, "Biped walking pattern generation by using preview control of zero-moment point," *IEEE Int. Conf. on Robotics and Automation*, 2003.

[19] T. Flash and N. Hogan, "The coordination of arm movements: an experimentally confirmed mathematical model," *Jrnl of neuroscience*, 1985.

[20] W. Hu, *et al.*, "Comparison study of nonlinear optimization of step durations and foot placement for dynamic walking," *IEEE Int. Conf. on Robotics and Automation*, 2018.